JOURNAL OF GEOPHYSICAL RESEARCH, VOL. 107, NO. A12, 1468, doi:10.1029/2002JA009430, 2002

NRLMSISE-00 empirical model of the atmosphere: Statistical comparisons and scientific issues

J. M. Picone, A. E. Hedin,[1] and D. P. Drob
E. O. Hulburt Center for Space Research, Naval Research Laboratory, Washington, D. C., USA

A. C. Aikin
Laboratory for Extraterrestrial Physics, NASA Goddard Space Flight Center, Greenbelt, Maryland, USA

Received 3 April 2002; revised 3 July 2002; accepted 8 August 2002; published 24 December 2002.

[1] The new NRLMSISE-00 empirical atmospheric model extends from the ground to the exobase and is a major upgrade of the MSISE-90 model in the thermosphere. The new model and the associated NRLMSIS database now include the following data: (1) total mass density from satellite accelerometers and from orbit determination (including the Jacchia and Barlier data sets), (2) temperature from incoherent scatter radar covering 1981–1997, and (3) molecular oxygen number density, $[O_2]$, from solar ultraviolet occultation aboard the Solar Maximum Mission. A new component, "anomalous oxygen," allows for appreciable O^+ and hot atomic oxygen contributions to the total mass density at high altitudes and applies primarily to drag estimation above 500 km. Extensive tables compare our entire database to the NRLMSISE-00, MSISE-90, and Jacchia-70 models for different altitude bands and levels of geomagnetic activity. We also explore scientific issues related to the new data sets in the NRLMSIS database. Especially noteworthy is the solar activity dependence of the Jacchia data, with which we study a large O^+ contribution to the total mass density under the combination of summer, low solar activity, high latitude, and high altitude. Under these conditions, except at very low solar activity, the Jacchia data and the Jacchia-70 model indeed show a significantly higher total mass density than does MSISE-90. However, under the corresponding winter conditions, the MSIS-class models represent a noticeable improvement relative to Jacchia-70 over a wide range of $F_{10.7}$. Considering the two regimes together, NRLMSISE-00 achieves an improvement over both MSISE-90 and Jacchia-70 by incorporating advantages of each. *INDEX TERMS:* 0355 Atmospheric Composition and Structure: Thermosphere—composition and chemistry; 0350 Atmospheric Composition and Structure: Pressure, density, and temperature; 0335 Atmospheric Composition and Structure: Ion chemistry of the atmosphere (2419, 2427); 0394 Atmospheric Composition and Structure: Instruments and techniques; 0358 Atmospheric Composition and Structure: Thermosphere—energy deposition; *KEYWORDS:* empirical, atmosphere, model, composition, temperature, drag

Citation: Picone, J. M., A. E. Hedin, D. P. Drob, and A. C. Aikin, NRLMSISE-00 empirical model of the atmosphere: Statistical comparisons and scientific issues, *J. Geophys. Res.*, *107*(A12), 1468, doi:10.1029/2002JA009430, 2002.

1. Introduction

[2] Empirical models of the thermosphere and mesosphere are an indispensable tool used by the operational and upper atmospheric research communities for data analysis, initialization of detailed physics-based models, and mission and instrument design. For over a decade, the empirical models of choice among upper atmospheric scientists have been the Mass Spectrometer Incoherent Scatter Radar (MSIS-class) models of composition, total mass density, and temperature: MSIS-86 [*Hedin*, 1987], which ranges upward from 90 km, and MSISE-90 [*Hedin*, 1991], which extends from the ground to the exobase. Several research communities continue to use the CIRA (1986) climatology, which consists of two overlapping specifications: tables generated from MSIS-86 for the thermosphere (altitude $z > 100$ km; see the discussion at http://nssdc.gsfc.nasa.gov/space/model/atmos/cospar2.html) and tables based on averages of global data compilations for the mesosphere and below ($z < 120$ km; see the discussion at http://nssdc.gsfc.nasa.gov/space/model/atmos/cospar1.html). Operational communities use the Jacchia-class models or in some cases, the more limited U.S. Standard Atmosphere (1976) (see the discussion at http://nssdc.gsfc.nasa.gov/space/model/atmos/us_standard.html). The database underlying operational Jacchia models (1970 and earlier) consists of total mass density derived from

[1] Also at Universities Space Research Association, Washington, D. C., USA.

0148-0227/02/2002JA009430

orbital decay of objects which flew during 1961–1970. Hedin based past MSIS-class models on over two decades of data on composition, temperature, and total mass density rather than on data on orbital dynamics.

[3] The new NRLMSISE-00 empirical atmospheric model is a major upgrade of the MSISE-90 model in the thermosphere and is now available for access and use by the scientific and operational communities (Appendix A4). This milestone fulfills our initial goal of preserving and continuing the line of MSIS-class empirical models. For estimating total mass density, the NRLMSISE-00 model is comparable to or better than the Jacchia-class models, since numerous orbital drag (F. Barlier, private communication to A. Hedin, 1985) and accelerometer data sets (F. Marcos, private communication) have been included in generating the model. A noteworthy addition to the NRLMSIS database is the actual orbital decay data on which the Jacchia models are primarily based. The model also incorporates recent data on temperature and molecular oxygen number density, $[O_2]$. The new data sets are extensive in size, spatial range, and the time period covered and represent significant departures from the MSIS database used to produce previous generations of the model.

[4] This upgrade is important because the MSIS and Jacchia models do not depend on calendar year and do not explicitly account for any gradual changes in the atmosphere due to anthropogenic or solar influences. The only way in which empirical models can reflect the recent state of the atmosphere is by our continually adding recent data to their databases and then modifying their parameter sets. In addition, instrumentation and data processing methods have improved and have become more diverse, potentially allowing the addition of higher-order terms and reducing the uncertainty of model coefficients. To accommodate new data, the formulation of the model and the methodology for generating it have become more robust (Appendix A).

[5] One change is particularly worthy of mention. The inclusion of drag data in our neutral atmospheric model has required us to account explicitly for an additional high-altitude drag component which is appreciable under some conditions and which is not in equilibrium at the thermospheric temperature. Limited studies have indicated that O^+ and hot atomic oxygen can contribute appreciably to drag for the combination of summer, high latitude, and high altitude (*Keating et al.* [1998] and section 4.1). As a result, the NRLMSIS formulation now explicitly includes a component called ''anomalous oxygen'' to account for the contribution of nonthermospheric species to satellite drag at high altitudes and permits the user to compute both the ''thermospheric mass density'' (or total neutral mass density) provided by past generations of MSIS and an ''effective'' mass density, which denotes the sum of the thermospheric mass density and the anomalous oxygen contribution at altitudes near the exobase.

[6] This paper compares the new model to the standard scientific (MSISE-90 [*Hedin*, 1991]) and operational (Jacchia-70 [*Jacchia*, 1970]) empirical models presently in use, through statistical comparison with the previous MSIS database and with the newly added data sets that make NRLMSISE-00 unique. We then address scientific issues related to the newly added data. Section 2 describes the newly added data sets and their relationship to the previous database. Section 3 presents statistical comparisons of NRLMSISE-00, MSISE-90, and Jacchia-70 with the NRLMSIS database. The statistical tables significantly augment a previous publication on drag and accelerometer data [*Hedin*, 1988]. Section 4 discusses important scientific issues related to the new data sets and model. Section 5 discusses our conclusions regarding NRLMSISE-00 and the direction of future development. Appendix A summarizes the formulation, generation, and access of the new model and addresses the use of orbital drag and accelerometer data to generate NRLMSISE-00.

2. NRLMSIS Database and Model

2.1. Relationship to Past Models

[7] NRLMSISE-00 retains the calling sequence and arguments of MSISE-90 and earlier MSIS models. As before, one can interpret the NRLMSIS model (for brevity, we will often exclude the designation ''E-00'') as a semiempirical ''view'' of its extensive underlying database covering several decades. That is, the model takes statistical variability into account while interpolating among, or extrapolating, the underlying data sets to estimate composition and temperature for times, geophysical conditions, and locations not covered specifically by the database. The model accomplishes this by fitting a set of parametric equations to the data, as described by Appendix A and references therein.

[8] As with earlier versions of the MSIS-class models, the NRLMSIS database includes ground-, rocket-, and satellite-based measurements. The data underlying MSISE-90 cover the period 1965–1983 and comprise incoherent scatter radar (ISR), mass spectrometer, solar ultraviolet (UV) occultation, pressure gauge, falling sphere, and grenade detonations. Until now, the database has not included either drag measurements, on which the Jacchia models were based, or satellite-borne accelerometer data. The new NRLMSIS upgrade includes these data sets.

[9] Both the MSIS and Jacchia models are sensitive to the level of geomagnetic activity and provide an estimate of the average upper atmospheric state under geomagnetic storm conditions. However, at high latitudes and high geomagnetic activity, available databases are sparse, and as statistical averages, the models do not capture the local structure and shorter timescales associated with any particular storm. The NRLMSISE-00 model remains a statistical average, but the database now contains more data covering extremes of location and forcing.

2.2. Expanded Database

[10] Recent data sets and new categories of data now augment the NRLMSIS database and model: (1) satellite drag [*Jacchia*, 1970; *Barlier et al.*, 1978; *Hedin*, 1988], orbit determination (1961–1973); (2) accelerometer [*Hedin*, 1988; F. Marcos, private communication, 1987], Atmosphere Explorer (AE-C, D, E) MESA [*Champion and Marcos*, 1973], Air Force SETA [*Rhoden et al.*, 2000], CACTUS [*Boudon et al.*, 1979], San Marco 5 [*Arduini et al.*, 1997]; (3) incoherent scatter radar, exospheric temperature (T_{ex}), Millstone Hill (1981–1997 [*Buonsanto and Pohlman*, 1998]), Arecibo (1985–1995 [*Melendez-Alvira et al.*, 1998]); (4) ISR, Lower thermospheric temperature

(T_{low}), Millstone Hill (1988–1997 *Goncharenko and Salah* [1998]); (5) Solar Maximum Mission (SMM) O_2 density data derived from occultation of solar UV emissions [*Aikin et al.*, 1993].

[11] The drag and accelerometer data on total mass density (ρ) remove a postulated deficiency of MSIS for orbital tracking applications. With the inclusion of the Jacchia data, the more extensive and well-documented NRLMSIS database should equal or improve the statistical predictions of ρ and of drag over those of the Jacchia models. We are testing this assertion by applying the model to operational precision orbit determination and prediction [*Knowles et al.*, 2001]. An important point is that the new data on total mass density could also influence the model coefficients for both temperature and composition. Such differences will become apparent as NRLMSIS is compared with additional data sets.

[12] The incoherent scatter radar data directly influence the model temperature, which is the core of the MSIS formulation. Because the new data are recent and cover an appreciable fraction of a solar cycle or more, these data are vital for both testing the existing models and producing new versions. The methods of processing ISR data have also undergone significant improvements over the last decade, increasing the quality of the inferred ionospheric properties [*Gonzalez and Sulzer*, 1996]. This imparts high value to our new data sets.

[13] The Millstone Hill data on lower thermospheric temperature (T_{low}) cover 100 km $\leq z \leq$ 130 km [*Goncharenko and Salah*, 1998]. In this atmospheric region, the neutral temperature is approximately equal to the ion temperature, so that extraction of the information is straightforward. These high-quality data permit us to check and reinforce key MSIS temperature model parameters. The data are also important in defining the model near the mesopause.

[14] The SMM mission provided data on the molecular oxygen number density [O_2] over the altitude range 140–220 km and over a wide range of solar activity. Prior to SMM, direct measurements of [O_2] above 150 km were not available at high solar activity. The SMM occultation measurements suggest that dissociation may increase sufficiently to keep this density nearly constant at 200 km as solar activity increases [*Kayser*, 1980; *Aikin et al.*, 1993]. These data are now part of the NRLMSIS database and are important in determining dependence on the solar extreme ultraviolet (EUV) flux and on magnetic activity. As a result, the data should be particularly useful in future analysis of EUV proxies developed recently [e.g., *Lean et al.*, 2001]. On the other hand, a longstanding conflict between mass spectrometer and solar UV occultation measurements of thermospheric [O_2] has had a profound effect on NRLMSIS because the occultation data do not follow diffusive equilibrium, corresponding to the thermospheric temperature $T(z)$, in the altitude range 140–220 km. This contradicts mass spectrometer data and MSISE-90 [*Aikin et al.*, 1993]. At the same time, the mass spectrometer data could be biased toward high values by recombination of atomic oxygen within the instrument. As an example, the two sources disagree on average by a factor of 2 or more at 200 km. The SMM data set has therefore required alterations in the formulation of NRLMSIS (see Appendix A) and has significantly influenced the dependence of [O_2] estimates on $F_{10.7}$ (section 4.2).

3. Statistical Comparisons of Models to Data

[15] A key component of this paper is the presentation of statistical measures to gauge the agreement of the commonly used empirical upper atmospheric models (MSISE-90 and Jacchia-70) and the new model, NRLMSISE-00, with the NRLMSIS database. In our discussion, angle brackets denote a weighted mean of the enclosed quantity. The weighting factor for a given data point is the squared reciprocal of the attributed error. For a data set $\{d_i\}$ and the corresponding model estimates $\{m_i\}$, we compute two factors: the weighted mean (β) of the residuals $\{d_i - m_i\}$, i.e., $\beta = \langle d_i - m_i \rangle$, and the corresponding standard deviation, $\sigma = [\langle (d_i - m_i)^2 \rangle - \beta^2]^{1/2}$. In a previous study, *Hedin* [1988] provided a visualization of these factors by plotting histograms of residuals of $\log_e \rho$, where ρ is the total mass density, for the Jacchia data set and the Jacchia-70 and MSIS-86 models. The histogram followed an approximate Gaussian shape, with a variance approximately equal to σ^2, as computed above, and with a median shifted from zero by our value of the mean residual (β).

[16] In the purest sense, the mean residual indicates the magnitude of systematic differences between a data set and corresponding model estimates. Positive β, or mean residual, indicates that a model underestimates the measured values on average. A negative mean residual signifies overestimation. The standard deviation measures the agreement between the geophysical variability contained in the model and the geophysical variability implicit in the NRLMSIS database. Interpretation of the standard deviation for a single model can be somewhat ambiguous, however, because σ also reflects noise in the data sets. In addition, if a model faithfully covers scales of true geophysical variability which have been filtered from the data, the computed σ of the model could be measurably larger than that of a less robust model which matches the spectral content of the data. This could happen, for example, with total mass density data derived from routine orbit (drag) determination, which filters the data on a timescale of days, while the MSIS-class models cover semidiurnal and terdiurnal timescales. For these reasons, we include baseline models for relative comparisons and we limit our conclusions to the particular data sets used: when multiple models are compared with identical data sets, the relative values of σ should indicate relative agreement of respective models with measured timescales and the associated phases inherent in the data.

[17] The NRLMSIS database consists of two components: the complete data sets acquired from the various sources and the subset of data "selected" to generate the model. *Hedin et al.* [1977] described the selection process, which was designed to ensure the widest coverage of the hyperspace of subroutine arguments (e.g., day of year, latitude, longitude) while satisfying constraints imposed by computing and storage limitations. The data selection method of Hedin et al. avoids dominance of the model coefficients by only a few large data sets, although this can also be accomplished by proper weighting of data-model residuals in computing χ^2. In order to insure against domination of NRLMSISE-00 by the new data sets and to

maintain consistency with past MSIS versions, we have performed a similar selection from the new data in generating the NRLMSIS model.

[18] The tables of (β, σ) values include both the model generation database and the complete, newly added data sets. For temperature T and data index i, the tables show a mean residual $\beta_T \equiv \langle T_i \text{ (data)} - T_i \text{ (model)} \rangle$ and a standard deviation $\sigma_T \equiv \{\langle [T_i \text{ (data)} - T_i \text{ (model)}]^2 \rangle - \beta_T{}^2\}^{1/2}$. For species number density $[x]$ and total mass density ρ, we have used log $[x_i]$ and log ρ_i as our respective primary statistical variables. We then express the mean residual for the mass density, i.e., $\langle \log_e \{\rho_i \text{ (data)}/\rho_i \text{ (model)}\} \rangle$, as a representative fractional density difference, $\beta_\rho = \exp \langle \log_e \{\rho_i \text{ (data)}/\rho_i \text{ (model)}\} \rangle - 1$. The corresponding standard deviation is $\sigma_\rho = [\langle \log_e{}^2 \{\rho_i \text{ (data)}/\rho_i \text{ (model)}\} \rangle - \log_e{}^2 (\beta_\rho + 1)]^{1/2}$. The equations for β_x and σ_x have the same form. Because the number of tables is large (27), they have been archived electronically for access by interested readers[1]. In the archive, we denote them as Tables 1a–1c through 9a–9c, where a, b, and c denote quiet ($Ap \leq 10$) and active ($Ap \geq 50$) geomagnetic conditions and the union of all geomagnetic conditions ("all" data), respectively. The tables abbreviate the names of the models to N00 (NRLMSISE-00), M90 (MSISE-90), and J70 (Jacchia-70) and cover total mass density (ρ), temperature, and individual species (excluding anomalous oxygen). For the tables relating to quiet conditions and to all data, the calculations used only data points deviating from the new model by 15 times the associated error, or less. For active conditions, the database was sufficiently sparse that all high-activity points were used to construct the tables. Finally, for "all" and $Ap \geq 50$, we used the 3-hour *ap* inputs to the NRLMSISE-00 ("N00") and MSISE-00 ("M90") models, while for quiet conditions, we used the daily *Ap* input.

[19] Even though the mean residual and standard deviation are coarse measures, they are useful for estimating model error. Both experimental noise and limitations in the temporal and spatial coverage of each data set can cause the relative values of β and σ to vary across data sources, potentially masking trends and systematic differences among models. Relative to our database (see the AGU archive), the most obvious differences among the models involve the standard deviation of the data-model residuals. Our most important observation is that NRLMSISE-00 is somewhat better than Jacchia-70 and MSISE-90 overall. For the data on total mass density (archive Tables 1a–1c), σ is comparable among the models, confirming the internal consistency of the drag/accelerometer data and the nondrag (composition and temperature) data. We reach the latter conclusion because the total mass density in MSISE-90 derives almost entirely from composition and temperature data, while Jacchia-70 derives entirely from drag and NRLMSISE-00 includes both data classes.

[20] As expected, NRLMSISE-00 and MSISE-90 show better results for composition than does Jacchia-70, especially as altitude increases (archive Tables 3–9). The comparable performance of NRLMSISE-00 and MSISE-90 for composition (except for $[O_2]$) also verifies that the extensive new data on total mass density have been added in a manner consistent with the prior MSIS representation of composition. The new SMM data have caused a shift in the mean value of $[O_2]$ in the lower thermosphere (section 4.2 and *Aikin et al.*, 1993]).

Table 1. Statistical Comparison of Empirical Models to Jacchia Data[a]

			N00		M90		J70	
Ap	Altitude, km	Points	Mean	SD	Mean	SD	Mean	SD
≤10	200–400	6,236	−0.06	0.17	−0.06	0.17	−0.04	0.17
	400–800	10,041	−0.07	0.23	−0.08	0.26	−0.07	0.25
	800–1200	5,586	0.01	0.23	0.03	0.27	−0.05	0.23
	>1200	15	0.20	0.09	0.27	0.10	−0.18	0.05
All	200–400	10,456	−0.07	0.17	−0.06	0.17	−0.07	0.19
	400–800	16,021	−0.08	0.25	−0.07	0.27	−0.09	0.28
	800–1200	9,373	0.01	0.24	0.04	0.27	−0.07	0.25
	>1200	24	0.22	0.12	0.30	0.11	−0.20	0.13
≥50	200–400	304	−0.05	0.23	−0.07	0.23	−0.12	0.25
	400–800	441	−0.01	0.36	0.01	0.39	−0.17	0.42
	800–1200	282	0.07	0.35	0.05	0.39	−0.14	0.39

[a]N00, NRLMSISE-00; M90, MSISE-90; J70, Jacchia-70. Mean, mean residual between data and model, expressed as a fraction of the model value; SD, standard deviation.

[21] Archive Tables 2a–2c show that the two MSIS models also agree better (than does Jacchia-70) with incoherent scatter radar measurements of exospheric temperature (which showed lower standard deviation values than did satellite data). For Jacchia-70, the best temperature results relative to the MSIS-class models occurred for the combination of lower altitudes and satellite-based observations, for which the three models had similar values of σ. At high geomagnetic activity, comparisons of all models with the data generally showed higher σ values than did the low geomagnetic activity cases. Also at high geomagnetic activity, the MSIS models showed lower σ values than did Jacchia-70.

[22] Considering key drivers of atmospheric variations makes the differences among models more apparent (e.g., see the next section on variations with the solar EUV flux, as represented by $F_{10.7}$). In addition, comparisons of the models for selected data sets are valuable, if the user has knowledge of those particular data sets, if the data sets come from the same or similar sources, or if particular altitude or geomagnetic activity ranges are emphasized. As an example and as an introduction to section 4.1 on anomalous oxygen contributions to total mass density, Table 1 compares the Jacchia data set to the three models. The table shows that the mean residuals (denoted "Mean") and standard deviations ("SD") of the three models are comparable in magnitude at low to moderate geomagnetic activity. However, two additional, secondary features appear. First, the Jacchia model shows a consistent negative mean residual (β), on average overestimating the Jacchia data at all altitudes, while NRLMSIS and MSISE-90 show a positive mean residual at high altitude and negative mean values at lower altitudes. Section 4.1 shows that this difference at high altitudes is likely attributable to a nonoptimal match of Jacchia-70 with the $F_{10.7}$ variability of the data. Second, at high geomagnetic activity, the standard deviations of the MSISE-90 and Jacchia-70 models are consistently higher than that of NRLMSIS. This suggests that the new model handles spatial and temporal variability somewhat better

[1] Supporting data tables are available via Web browser or via Anonymous FTP from ftp://kosmos.agu.org, directory "apend" (Username = "anonymous", Password = "guest"); subdirectories in the ftp site are arranged by paper number. Information on searching and submitting electronic files is found at http://www.agu.org/pubs/esupp_about.html.

than the other models at elevated geomagnetic activity. In addition, at high geomagnetic activity, the mean residual of the Jacchia-70 model is noticeably larger than the residuals of the MSIS models, indicating that the former systematically overestimates the data.

4. Scientific and Technical Issues

4.1. Anomalous Oxygen and Solar Activity

4.1.1. Background

[23] An important addition to the NRLMSIS model is an ''anomalous oxygen'' component to high-altitude drag and total mass density at the summer high latitudes. At high altitude (>500 km), this component augments the ''thermospheric'' total mass density attributable to the neutral species in diffusive equilibrium at the thermospheric temperature T, including atomic hydrogen and helium (Appendix A). The anomalous oxygen component accounts for the presence of appreciable hot atomic oxygen (O_h) or atomic oxygen ions (O^+) near the exobase under some conditions but does not explicitly distinguish contributions by the two species. As described below, observational evidence is sufficient to warrant this additional component to drag. Presently, we lack the detailed knowledge about the two species (O_h, O^+) to account for their individual effects. Although cited studies of hot oxygen near the exobase have some results in common, the experimental characterization of hot atomic oxygen in this region is noticeably incomplete. Likewise, only recently did *Keating et al.* [1998] demonstrate that an appreciable O^+ component to high-altitude drag can exist. Also important was their finding that the mass density attributable to other ionic species (e.g., H^+, He^+) was minor in relation to O^+ under the conditions studied.

[24] Analyses of data and empirical models by *Hedin* [1989] led him to infer an additional nonthermospheric oxygen component to the total mass density near the exobase. In particular, he found that an appreciable hot atomic oxygen population could be present under the combination of high latitude and high altitude (>600 km) in the summer hemisphere. For this region of the atmosphere, during high solar activity, Hedin observed an elevated atomic oxygen population by comparing the MSIS-86 model to high-altitude data from the neutral mass spectrometer aboard Dynamics Explorer 2 (DE 2). The latter enhancement was consistent with the detection of a hot oxygen geocorona by *Yee et al.* [1980] during solar maximum with temperature of ~4000 K.

[25] For low to moderate solar activity, also for the combination of high altitude, high latitude and summer, the Jacchia-70 model showed significantly higher total mass density (and helium concentration) than did MSIS-86. Given the corresponding result of the DE 2 analysis for high solar activity, Hedin suggested that the Jacchia-70 enhancement in total density at lower solar activity (and the accompanying discrepancy in helium concentration) could be caused by an appreciable hot atomic oxygen geocorona under those conditions.

[26] Recent analyses of ISR data from Millstone Hill by *Oliver* [1997] and *Oliver and Schoendorf* [1999] (emphasizing altitudes around 400 km) have indicated that a small, but nonnegligible, hot oxygen component can account for a theoretical deficit in ion heating in the upper thermosphere. According to these studies, the hot oxygen component would be especially important, for example, at night, at the solstices, and during solar minimum. *Schoendorf et al.* [2000] have developed model profiles of hot oxygen for use in deriving T_{ex} from ISR data (section 4.3). A broadening of the investigations by Oliver et al. will augment the present understanding of the hot oxygen component and could guide our future upgrades of NRLMSIS.

[27] Meanwhile, the exclusive emphasis on a hot atomic oxygen component to drag changed when *Keating et al.* [1998] analyzed neutral and ion mass spectrometer measurements aboard the Midcourse Space Experiment (MSX). MSX flew in a Sun-synchronous (near-polar) circular orbit at approximately 900 km during the most recent solar minimum. Similar to Hedin, Keating et al. observed discrepancies in the respective Jacchia-70 and MSIS-86 estimates of [He] and total mass density as MSX transited the summer pole. Under these conditions, the MSX neutral composition data showed that the Jacchia-70 model incorrectly attributes its elevated mass density (relative to MSIS-86) to higher values of [He]. Keating et al. then found that the O^+ density measured by MSX accounted for the higher mass density implied by Jacchia-70 near the summer pole at 900 km under solar minimum conditions. Keating et al. also found that the mass density attributable to other ionic species (e.g., H^+, He^+) was minor in relation to O^+ under the conditions studied.

[28] In response to these developments, the NRLMSIS model now includes an ''anomalous oxygen'' (AO) component, which represents any appreciable, persistent nonthermal species (thought to be O^+ or hot O populations) at higher altitudes (>500 km). The functional form of the anomalous oxygen model profile is similar to that of an isothermal Chapman layer, with an adjustable magnitude and scale height (or temperature; Appendix A1). The data used to evaluate these parameters were the drag data sets of Jacchia and Barlier (JB) (section 2.2) above 600 km. At the same time, we excluded the summer JB data above 600 km from the data sets used to determine the He and ''thermospheric'' O components of the model. (The term ''thermospheric'' O represents the atomic oxygen population in equilibrium at the thermospheric temperature T). While the winter JB data above 600 km have been used to generate coefficients for He, thermospheric O, and anomalous O, comparisons of NRLMSISE-00 and MSISE-90 to these data have shown only small differences. We conclude that the anomalous oxygen component has influenced the new model far less during winter at high altitudes. Surprisingly, the Jacchia-70 model agrees less well with the Jacchia data than do the MSIS models under such conditions (next subsection).

[29] Our anomalous oxygen data set does not include the high-altitude, spin mode DE 2 neutral mass spectrometer data [*Hedin*, 1989] for a combination of reasons:

1. The drag data should account for both O^+ ions and hot O atoms, while the DE 2 data account only for the neutral atoms. Therefore the DE 2 data could bias the fit against the O^+ component of the drag data.
2. Retrieving the hot oxygen component of DE 2 data is dependent on using a model for the cold oxygen component.
3. The DE 2 data have further limitations: a small number of points (425) above 600 km, covering only high solar activity (81-day average, $\langle F_{10.7} \rangle \geq 190$) and a narrow temporal range (fall–winter of 1981–1982).

[30] Fortunately, a comparison of the Jacchia-Barlier data to the DE 2 data for high latitudes and elevated solar activity ($\langle F_{10.7} \rangle > 150$) shows good qualitative agreement, indicating that the drag-based data set has captured the elevated neutral density implied by DE 2. A tantalizing result is that the fit of the NRLMSIS anomalous oxygen component to the high-altitude Jacchia-Barlier total mass density data yielded an effective temperature of approximately 4177 K ± 3%. We do not hold this to be definitive, given the limitations of our high-altitude drag data set, and we have therefore chosen to maintain this parameter at 4000 K, in line with previously cited references on hot oxygen. Note that such a temperature would seem to be too high for oxygen ions to form the primary component of our anomalous oxygen model. Clearly, we need more data on (and modeling of) neutral and ionized atomic oxygen at high altitudes to develop a faithful representation of the total mass density near the exobase.

4.1.2. Comparison of Empirical Models With High-Altitude Jacchia Data

[31] Comparison of empirical models with the Jacchia data above 600 km reveal both anticipated and unexpected features. First, the high-altitude Jacchia data support the observations of *Keating et al.* [1998], regarding a significant enhancement in total mass density over past MSIS-class models, for the combination of low solar activity, high altitude, and high summer latitude. However, this difference decreases rapidly with increasing $F_{10.7}$ and decreasing altitude, and surprisingly, the Jacchia-70 model significantly overestimates the observed density at very low $F_{10.7}$. Further, as a function of $F_{10.7}$ under the corresponding winter conditions, MSIS-class models generally agree better with the Jacchia data than does the Jacchia-70 model itself. As a result, NRLMSISE-00 achieves improvements over both MSISE-90 and Jacchia-70, incorporating advantages of each.

[32] Figures 1 and 2 compare the (previous day) $F_{10.7}$ dependence of the total mass density from four sources: (1) the Jacchia data set on total mass density (data denoted here by ρ_d), (2) the corresponding NRLMSISE-00 model values (ρ_N), (3) the MSISE-90 model values (ρ_M), and (4) the Jacchia-70 model values (ρ_J). Because the Jacchia models are the standard of the astrodynamics community for estimating orbital drag, we normalize all density values to the Jacchia-70 model. The figures therefore depict bin-averaged differences of natural logarithms, $\log_e (\rho_N/\rho_J)$ denoted by solid lines, $\log_e (\rho_M/\rho_J)$ denoted by dashed lines, and $\log_e (\rho_d/\rho_J)$, located at the centers of the $\pm 1\sigma$ vertical bars (σ, standard deviation). The averaging bins are $10F_{10.7}$ units, and both abscissas and ordinates are bin-averaged values. The number at the center of a vertical bar is the approximate base 2 logarithm of the number of points in the corresponding bin. The solid horizontal line at an ordinate of 0.0 represents the bin-averaged Jacchia-70 values. When a vertical bar is approximately centered on the horizontal line, the Jacchia-70 model is in good agreement with the data in the given bin. Significant displacement of a vertical bar from the horizontal line signifies poor performance by Jacchia-70.

[33] Figure 1a shows the solar activity dependence of ρ above 900 km for the combination of summer and high latitudes ($|\theta| \geq 45°$); the MSX data of *Keating et al.* [1998] correspond to (previous day) $F_{10.7} = 71$, altitude $z = 900$ km, and $\theta = 80.6°$N. For low to moderate solar activity ($F_{10.7} \in [75, 175]$), the Jacchia-70 model captures the trend and magnitude of these data somewhat better than does NRLMSISE-00. A comparison to MSISE-90 verifies the enhancement observed by Keating, but this effect diminishes as $F_{10.7}$ approaches 130. Unexpectedly, as $F_{10.7}$ decreases below 75, the Jacchia-70 model overestimates the total measured mass density by an increasing amount. In fact, below $F_{10.7} \sim 75$, NRLMSISE-00 appears to agree with the Jacchia data better than does Jacchia-70, while above ~130 the differences between the two models are relatively minor.

[34] For the entire data subset containing 684 points, we also compare statistical measures: mean residual $\beta \equiv \langle \log_e (\rho_d/\rho_{\text{model}}) \rangle$ and standard deviation $\sigma = [\langle \log_e{}^2 (\rho_d/\rho_{\text{model}}) \rangle - \beta^2]^{1/2}$, where "model" signifies NRLMSISE-00, MSISE-90, or Jacchia-70. Brackets indicate a weighted average over the data subset, and the weight of each datum in both averages is the squared reciprocal of the error attributed to the datum. The values of (β, σ) are (−0.08, 0.22) for NRLMSISE-00 and (−0.10, 0.24) for Jacchia-70, implying no particular advantage to either model, in spite of the differences in Figure 1a. MSISE-90 has (β, σ) = (0.19, 0.29), indicating a systematically low average density estimate and a poorer match with the observed $F_{10.7}$ dependence.

[35] Figure 1b shows the situation for Jacchia's data set during summer at high latitudes in the altitude range 600–900 km (1085 points). Comparisons with MSISE-90 show that the effect observed by Keating et al. has decreased considerably in magnitude and occurs over a narrower range of $F_{10.7}$ values. Moreover, NRLMSISE-00 agrees better with the dependence of the data on $F_{10.7}$ than does Jacchia-70 and agrees especially well with the data at low solar activity. The statistical measures are (β, σ) = (−0.08, 0.25) for NRLMSIS versus the Jacchia-70 values of (−0.02, 0.31). MSISE-90 has values of (0.05, 0.34), primarily due to poorer agreement at low solar activity. Notice that the mean residual (β) values of the models do not reflect the striking differences in dependence on $F_{10.7}$ and actually attribute a modest advantage to Jacchia-70, while σ gives a coarse indication that NRLMSISE-00 does a better job representing the $F_{10.7}$ dependence of the data.

[36] In winter, for the same combination of latitude and altitude, the MSIS-class models generally outperform Jacchia-70 when they are compared with the Jacchia data set as a function of $F_{10.7}$. Figure 2a, for $z \geq 900$ km (505 points), shows that the Jacchia model gives somewhat better agreement at low $F_{10.7}$ but varies oppositely with the data as $F_{10.7}$ increases. At $F_{10.7} \approx 98$, the NRLMSIS and MSISE-90 models do show a 45% overestimate, but this is based on only two data points. In fact, for $F_{10.7}$ in the range 80–120, only 19 data points were available, making the low $F_{10.7}$ range difficult to evaluate. Across the entire range of solar activity, the differences among models are apparent in the mean residuals: (β, σ) = (−0.06, 0.19) for NRLMSISE-00 and (−0.12, 0.20) for MSISE-90 versus the Jacchia-70 values of (−0.24, 0.15).

[37] Figure 2b, for $z = 600$–900 km (1449 points), shows similar but less extreme differences in mean residual, with (β, σ) = (−0.14, 0.19) for NRLMSISE-00, (−0.22, 0.21) for MSISE-90 and (−0.20, 0.20) for Jacchia-70. The β values

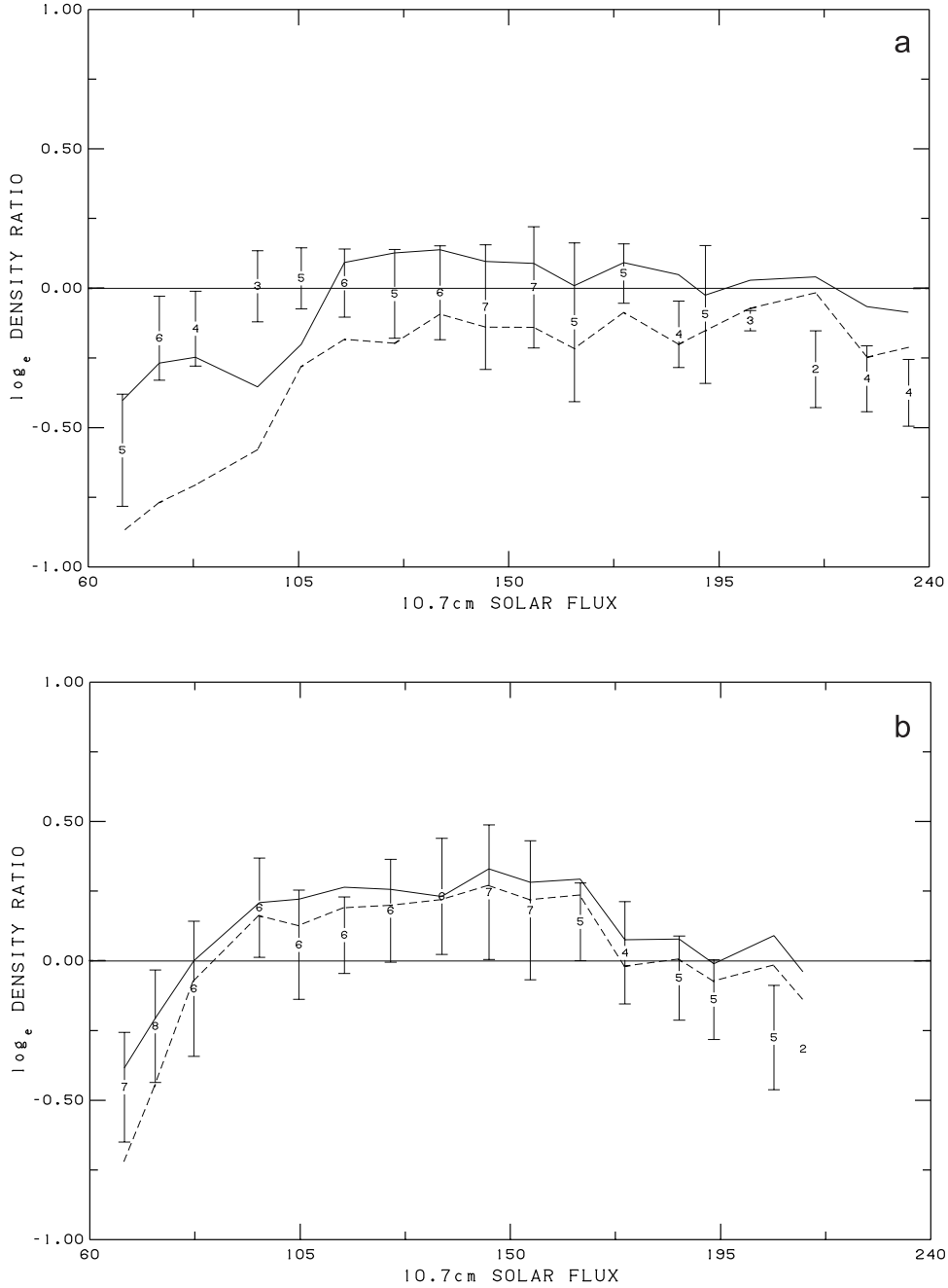

Figure 1. Natural logarithm of total mass density (data and model values) versus previous day $F_{10.7}$ for the combination of summer, high latitudes, and high altitudes: (a) $z \geq 900$ km and (b) 600 km $\leq z \leq 900$ km. The density values are normalized to the Jacchia-70 model and are averaged in bins of 10 $F_{10.7}$ units. Vertical bars correspond to the $\pm 1\sigma$ range of Jacchia data within each bin; the Jacchia-70 model values fall on the horizontal line at 0.0. The number at the center of a vertical bar is the approximate base 2 logarithm of the number of points in the corresponding bin. NRLMSISE-00 corresponds to the solid curve and MSISE-90 to the dashed curve.

are closer primarily because the number of data points decreased with increasing $F_{10.7}$, for which the deviation of Jacchia-70 from the Jacchia data was also increasing.

[38] The respective β and σ values for NRLMSISE-00 and Jacchia-70 are similar, especially for the cases in Figure 1, demonstrating that statistical averaging can mask qualitative differences. Such filtering of model estimates by averaging over one or more arguments might explain the comparable performance of MSISE-90 and Jacchia-70 for "special perturbations" (SP) orbit determination [*Marcos et al.*, 1998]. An operational SP calculation fits a detailed numerical propagator, which includes an atmospheric drag term, to space object observations that occur over a "fit span" of several days. The fitting process acts to filter the density model over several days [*Neal et al.*, 1998]. In addition, one of the fitting parameters is the "inverse

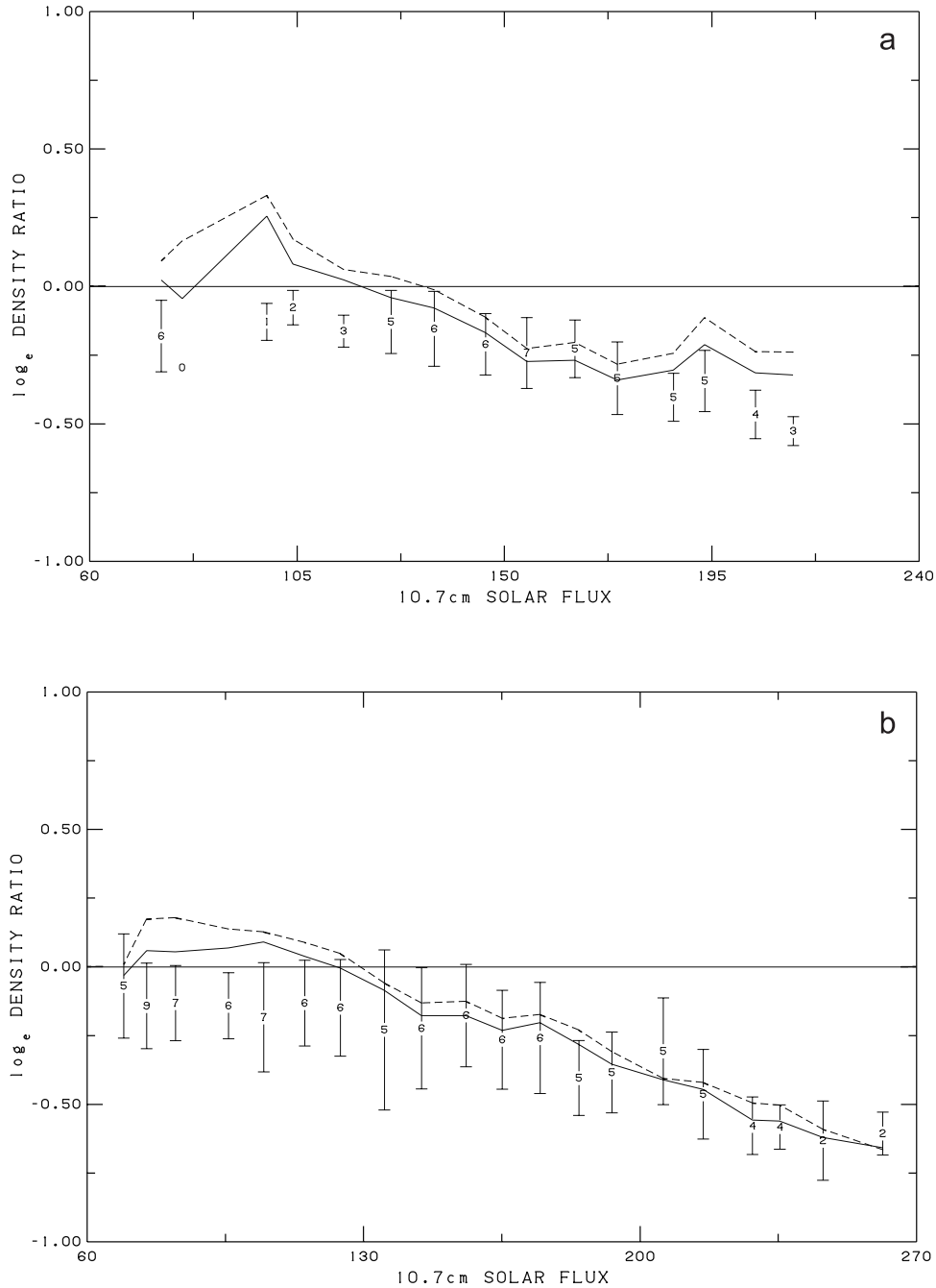

Figure 2. Same as Figure 1 for the combination of winter, high latitudes, and high altitudes: (a) $z \geq 900$ km and (b) 600 km $\leq z \leq$ 900 km.

ballistic coefficient," which multiplies the atmospheric density in the drag term. Adjusting the ballistic coefficient corrects the model bias over the fit span [*Marcos et al.*, 1998]. On the other hand, the detailed differences among models are of great importance in orbit prediction, for which no observations of the space object are available.

4.2. Solar Ultraviolet Occultation Versus Mass Spectrometry

[39] We have included the UV occultation observations of $[O_2]$ from the Solar Maximum Mission [*Aikin et al.*, 1993] in generating the new model. We have also added UV occultation data derived from a second band (channel 19) on the AE-E EUVS instrument. Aikin et al. show that as altitude increases within the range 140–220 km, solar occultation observations of $[O_2](z)$ fall below the diffusive equilibrium values by an increasing amount. In contrast, both mass spectrometer data and the MSISE-90 profiles of $[O_2](z)$ are in approximate diffusive equilibrium above ~150 km [*Meier et al.*, 2001]. This conflict between the two experimental techniques adds to a longstanding controversy [*Aikin et al.*, 1993, and references therein]. As is discussed below, these differences increase with solar activity.

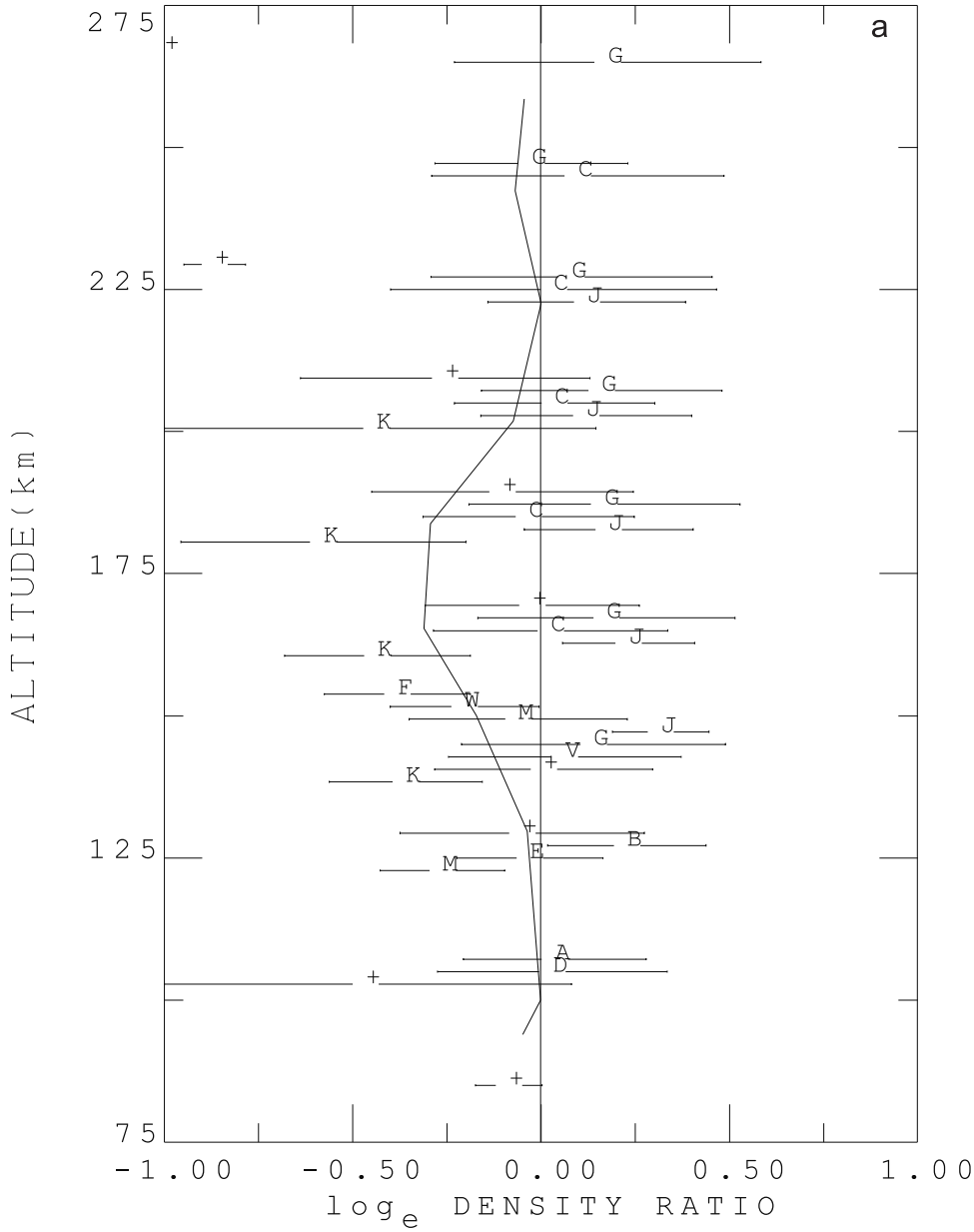

Figure 3. (a) Lower thermospheric profile of $[O_2]$: $\log_e$ of ratio to MSISE-90 values. Vertical averaging interval, 20 km. Solid curve, NRLMSISE-00 values. Letters and symbols identify individual data sources (AE, Atmosphere Explorer missions; SMM, Solar Maximum Mission). Solar ultraviolet occultation: (K) SMM; (A) AE-C, 100 km; (B) AE-C, 130 km; (V) AE-C, 150 km; (D) AE-E, 100 km; (E) AE-E, 130 km; (F) AE-E, 150 km, channel 19; (W) AE-E, 150 km, channel 6; (M) rocket. Mass spectrometer: (C) AE-C, (G) AE-D, (J) AE-E. Plus signs, rocket. (b) Natural logarithm of lower thermospheric $[O_2]$ versus 81-day mean $F_{10.7}$, averaged within bins of 10 flux units. The plot shows the bin-averaged data values normalized by MSISE-90. Vertical bars correspond to the $\pm 1\sigma$ range of normalized $[O_2]$ values within each bin. MSISE-90 corresponds to the horizontal line at 0.0. (c) Same as Figure 3b, but with data normalized to NRLMSISE-00, which corresponds to the horizontal line at 0.0.

[40] The SMM UV data show much weaker solar activity dependence than do the mass spectrometer data [*Aikin et al.*, 1993]. As a result of these differences, we have modified the parameterization of the lower thermospheric altitude profiles of O_2 and O to allow more flexibility in NRLMSISE-00, as described in Appendix A. The model now accounts for solar activity dependent departures from diffusive equilibrium in the lower thermosphere. Figure 3a shows that the new model is a statistical compromise between the two data sources in the altitude region 125–225 km covered by the SMM data. Above this region the NRLMSIS $[O_2]$ profile approaches diffusive equilibrium.

[41] Figure 3b shows the dichotomy between the newly added data and the previously existing data, from which the MSISE-90 model (horizontal line at 0.0) was generated. The low-altitude AE-E UV occultation data (labeled D and E)

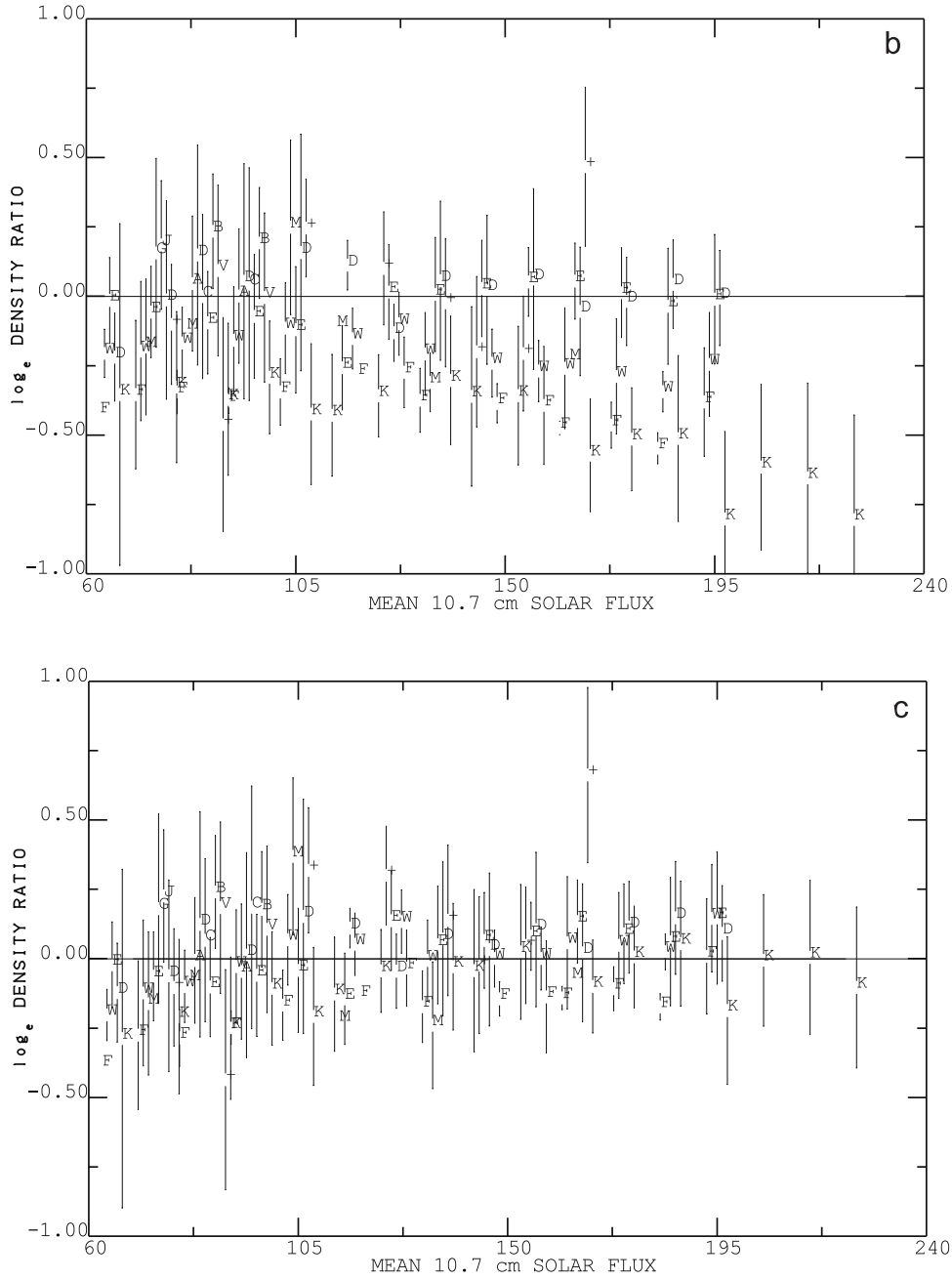

Figure 3. (continued)

extended the solar activity dependence of the MSISE-90 database. These data are reasonably consistent with MSISE-90, with mass spectrometer data, and with low-altitude, low $F_{10.7}$ AE-C UV occultation data (Figure 3a and *Aikin et al.* [1993]). In contrast, the newly added SMM data and the rocket and AE-E UV occultation data at 150 km (labeled K, M and F and W, respectively) differ noticeably from the MSISE-90 model, although these data appear to be consistent with each other. Figures 3a and 3b show that the magnitude of the disagreement depends on both altitude and $F_{10.7}$, as indicated above.

[42] Figure 3b also verifies that the SMM $[O_2]$ data depend less strongly on $F_{10.7}$ than does MSISE-90, which did not include those data. Figure 3c demonstrates that the new NRLMSISE-00 model fits the $[O_2]$ database far better than MSISE-90, primarily because of the adjustment to the altitude profile in the region of transition from a fully mixed state to diffusive equilibrium (Appendix A).

[43] The accuracy of both mass spectrometry and solar UV occultation remains an open question. Further improvement of the NRLMSIS model of $[O_2]$ in the lower thermosphere awaits a resolution of the differences between the two major data classes (i.e., observational techniques). This also affects the model atomic oxygen ([O]) profile in the lower thermosphere, where our primary source of information on [O] is mass spectrometer data on total oxygen number density, $[O] + 2[O_2]$. Appendix A (section A1.1) describes the new representation of $[O_2](z)$ and $[O](z)$ that

we use to accommodate the effects of SMM data on NRLMSISE-00. Comparison of the new model with our total oxygen data shows some evidence of slight improvements, for example, in variation with mean $F_{10.7}$. On the more limited basis of statistical measures (mean residual and standard deviation), the new model is quite similar to MSISE-90 vis-à-vis our data on total oxygen content in the thermosphere.

[44] On the other hand, the molecular oxygen number density, $[O_2]$, is noticeably lower in NRLMSISE-00 throughout the thermosphere and over a broad range of $F_{10.7}$ values. This has consequences also for the model's O_2 mixing ratio in the mesosphere, as compared with that of MSISE-90 (Appendix A section A1.2.2). Because the MSIS-class models are entirely empirical and the NRLMSIS database is presently devoid of direct data on $[O_2]$ in this region, a credible synoptic-scale representation of mesospheric $[O_2]$ awaits the addition of appropriate data to the database.

[45] Numerical model studies of this problem have been limited [*Aikin et al.*, 1993]. *Meier et al.* [2001] recently analyzed a general circulation model calculation at moderate solar activity and low geomagnetic activity which departs from diffusive equilibrium in the lower and middle thermosphere, unlike MSISE-90. However, the larger problem of solar activity dependence remains to be addressed by using detailed three-dimensional models [*Aikin et al.*, 1993].

4.3. Exospheric Temperature

[46] The Millstone Hill and Arecibo incoherent scatter radar data on exospheric temperature (T_{ex}) are of high quality and extend the NRLMSIS database well into the 1990s. These data result from fitting a model of ion heat balance and chemistry to the ion temperature profile ($T_i(z)$), using ISR observables and parameterized models of neutral oxygen and temperature [e.g., *Buonsanto and Pohlman*, 1998]. The retrieval of T_{ex} from the ISR data did not include a hot oxygen component [*Schoendorf et al.*, 2000]. The newly added Millstone Hill data, shown in Figure 4a, cover the period 1981–1997. The data include the June 1991 geomagnetic storm with maximum $\{F_{10.7}, ap\} \sim \{250, 300\}$ (see *Litvin et al.* [2000] and references therein) and another period around 29 October 1991 with maximum $\{F_{10.7}, ap\} \sim \{270, 235\}$. Litvin et al. pointed out that during the most intense storm period of June 1991, molecular ions dominated the chemistry, requiring a modification in the algorithms used to retrieve T_{ex} ; a similar situation apparently occurred in late October. Even after this correction, however, T_{ex} ranged significantly below the predictions of MSISE-90 for both periods. In fact, given that the difference was greater in October 1991, when $F_{10.7}$ was higher (Figure 4a, abscissa ~275), the elevated $F_{10.7}$ might also be a factor in the lower value of T_{ex}.

[47] Figure 4b shows the variation of the new Arecibo ISR data with previous day $F_{10.7}$; these data also include periods of high geomagnetic activity, with some daily *Ap* values well over 50. Interestingly, MSISE-90 provides a somewhat better fit at high solar activity ($\geq$240) than does NRLMSISE-00, suggesting that the response to solar forcing might vary with latitude. Unfortunately, relatively few data points are available at such high values of $F_{10.7}$, and the database has not supported retrieval of a meaningful latitude-$F_{10.7}$ coupling term (Appendix A, *Hedin* [1987]). Indeed, no clear statistical advantage for either model emerges from comparison with the entire Arecibo data set on upper thermospheric temperature, which extends over the last 35 years.

[48] The findings by Millstone Hill under elevated geomagnetic activity in 1991 led naturally to a search for Arecibo measurements that intersected with Millstone Hill data during 1991. Two such periods occurred early in the year (mid-January and mid-March). At those times, $F_{10.7}$ was high (180–275) while *Ap* was low to moderate (<35). During these periods, the mean temperature residual (β_T) relative to NRLMSISE-00 had the same sign at both ISR sites: negative for mid-January, with $F_{10.7} \sim 180–220$, and positive for mid-March, when $F_{10.7} \sim 240–275$. The respective mean residuals were also similar in magnitude, though 20–40% less than the β_T values for Millstone Hill during the June and October storm periods. The similarity of β_T values at the two sites during moderate geomagnetic activity hints at a global error source in the model. An example is the use of $F_{10.7}$ as a proxy for the solar EUV flux, which drives variability of the thermospheric density on timescales of a day or longer. *Marcos et al.* [1998] and *Rhoden et al.* [2000] have used drag and accelerometer data, respectively, to explore other proxies as candidates to augment or replace $F_{10.7}$. The differing signs of the mean residuals (β_T) during these moderate geomagnetic activity periods is characteristic of comparisons between data and approximately unbiased models, contrasting with the decidedly negative β_T values observed during middle and late 1991 when maximum *ap* was very high.

[49] Most importantly, the new ISR and total mass density data, when combined with the previous MSIS data sets, have changed the solar activity dependence of the temperature in NRLMSISE-00 relative to that of MSISE-90 (and MSIS-86), especially at higher altitudes. Figure 5 shows the difference in mean exospheric temperature estimates produced by the models as a function of latitude and $\langle F_{10.7} \rangle$. The NRLMSISE-00 T_{ex} is above that of MSISE-90 only at low latitudes and for moderate to low $\langle F_{10.7} \rangle$ and then by only a few degrees. As solar activity increases above moderate values, the NRLMSISE-00 value of T_{ex} falls below that of MSISE-90 by a steadily increasing amount, reaching −40 K at $\langle F_{10.7} \rangle > 220$ and high latitudes, $|\theta| > 45°$. This difference is less pronounced at lower latitudes, as we might expect from Figure 4b. The mean total mass density behaves similarly to the temperature. Inspection of the individual NRLMSISE-00 data sets on composition, temperature, and density have generally confirmed this behavior.

5. NRLMSIS Model: Present and Future

[50] The new database underlying the NRLMSISE-00 model incorporates data on total mass density (orbital drag and satellite accelerometers), recent incoherent scatter radar observations covering more than a solar cycle, and satellite-borne FUV occultation measurements of $[O_2]$ from SMM. The model interpolates among newly added and past data sets, often incorporating new features or strengths of each data set. As a result, the exospheric temperature in

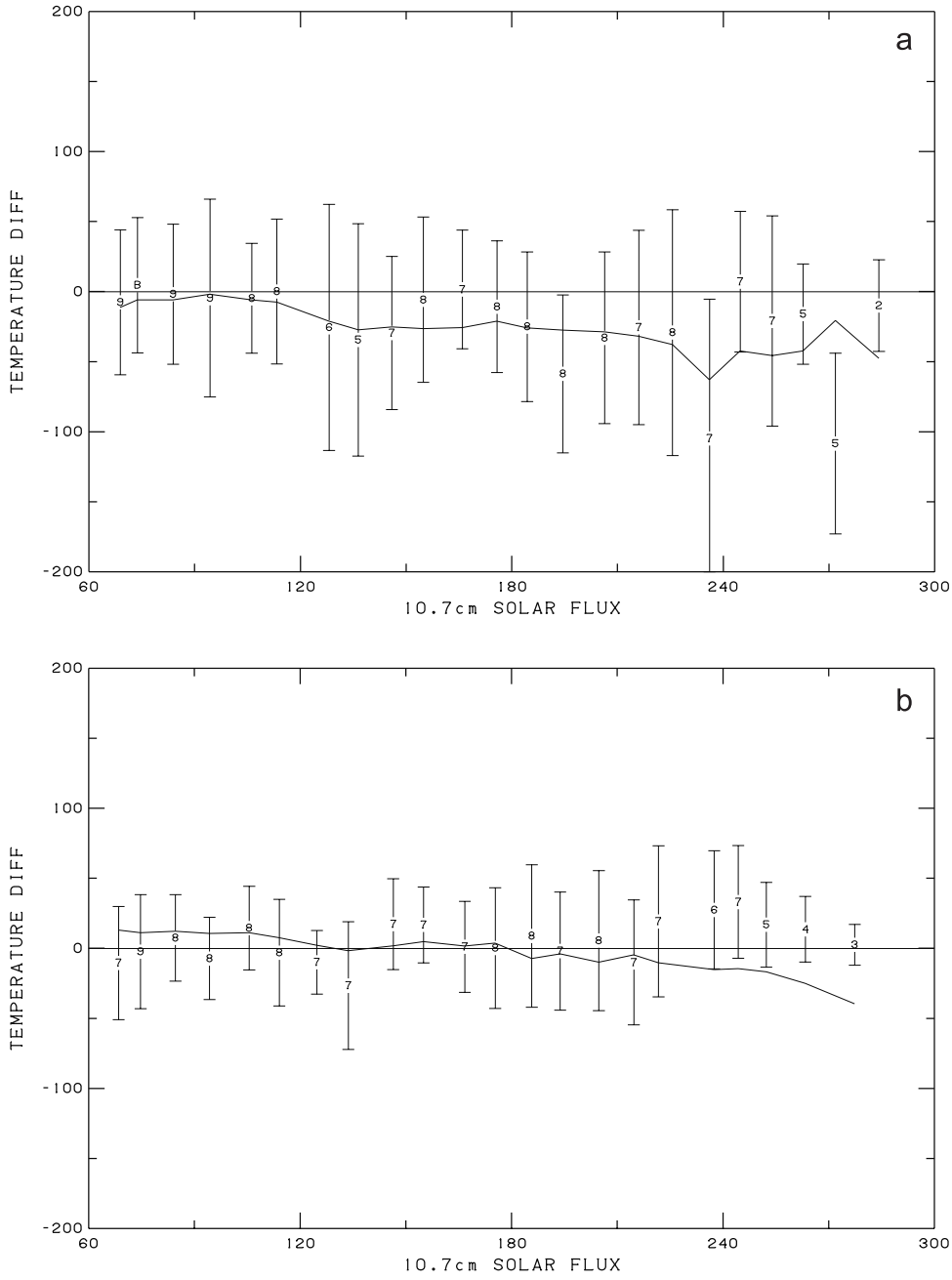

Figure 4. T_{ex} versus $F_{10.7}$ (previous day), averaged over bins of 10 flux units: (a) Millstone Hill data (1981–1997) and (b) Arecibo data (1985–1995). The quantities plotted are differences of data (vertical bars) and of NRLMSISE-00 model values (solid curve) from MSISE-90 (horizontal line at 0.0).

NRLMSISE-00 now shows somewhat weaker dependence on $F_{10.7}$ relative to MSISE-90. In the lower thermosphere, the model provides a statistical compromise between mass spectrometer and solar ultraviolet occultation data in terms of the altitude dependence of $[O_2]$ but follows the weaker solar activity dependence of UV occultation data more closely.

[51] The incorporation of satellite-based data on total mass density has allowed the inclusion of a new component (anomalous oxygen) to correct the model estimates of total density at high altitudes (near the exobase). This recognizes the conclusion of *Keating et al.* [1998] that O^+ can dominate drag under particular conditions and, through similar analysis, the conclusion of *Hedin* [1989] that hot oxygen could be important to drag. Comparison of NRLMSIS and the standard operational and scientific models to the orbit-based data of Jacchia at high altitudes has revealed significant differences in the seasonal and solar activity dependence of the models. The new model appears to provide advantages over both Jacchia-70 and MSISE-90 for estimating total mass density.

[52] The broadening of the database, along with comments by users and plans to replace or augment the $F_{10.7}$ input with a better proxy for the solar chromospheric extreme ultraviolet (EUV) flux, has led to modifications in the model formulation (see Appendix A for details).

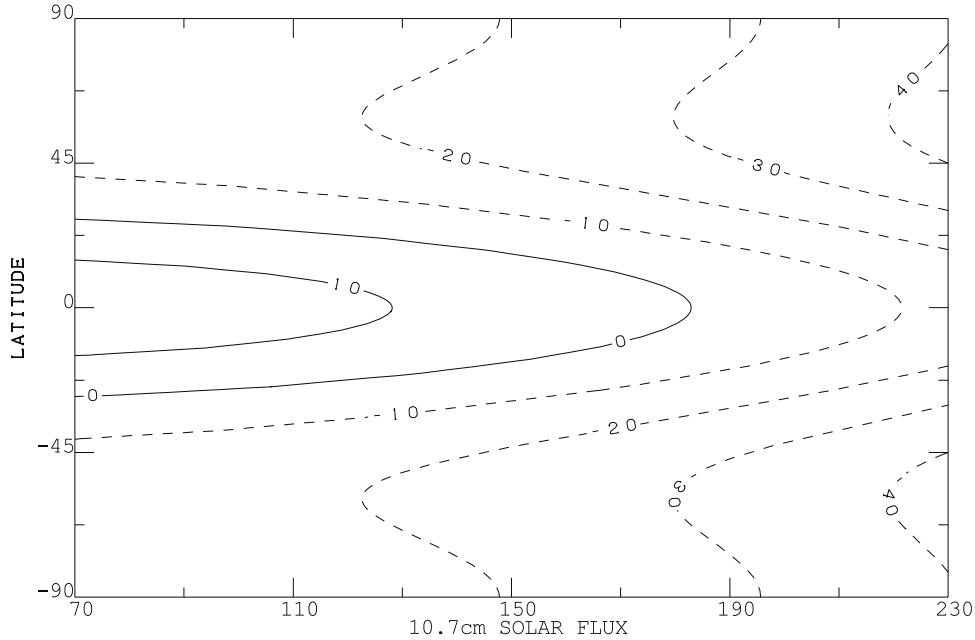

Figure 5. Exospheric temperature difference between NRLMSISE-00 and MSISE-90, averaged over longitude and time, as a function of latitude and $\langle F_{10.7} \rangle$. Solid contours are positive and dashed contours are negative.

1. A new coupling term between previous day $F_{10.7}$ and mean $F_{10.7}$ (Appendix A1) permits more flexibility in representing the dependence on solar EUV.

2. An anomalous oxygen model in the upper thermosphere allows for increased drag under some conditions.

3. The upgraded representation of $[O_2](z)$ in the lower thermosphere allows more general and higher-altitude departures from diffusive nonequilibrium and weaker solar activity dependence [*Aikin et al.*, 1993].

4. A new $[O](z)$ parameterization in the lower thermosphere compensates for changes in the new representation of $[O_2](z)$, primarily when fitting mass spectrometer data on total oxygen content, $[O] + 2[O_2]$.

5. The hydrostatic equilibrium constraint extends over a wider altitude range to tie the upper and lower atmospheric regions together self-consistently (Appendix A2).

6. The thermal diffusion factor for Ar is now nonzero.

[53] In connection with item 5, Appendix A1.2 points out that NRLMSISE-00 produces a temperature structure similar to a mesosphere inversion layer (MIL) under some conditions (e.g., equatorial region at night, low latitudes). When relevant satellite- and ground-based data are added to the database, the next generation NRLMSIS model could potentially provide a useful climatology of MILs.

[54] An underlying theme of this paper and of our future work is the dependence of the upper atmosphere on the solar EUV flux, which is the primary driver on timescales of a day or longer. Section 4 shows that the dependence on the $F_{10.7}$ solar EUV proxy is different for the respective empirical models favored by operational and scientific communities. The new NRLMSISE-00 model appears to incorporate advantages of both model classes and therefore helps to close the gap between these models. In addition, the atmospheric calibration method of *Marcos et al.* [1998] and a follow-on implementation in terms of ultraviolet remote sensing use near-real-time atmospheric data to improve density estimation for the "present" epoch [*Nicholas et al.*, 2000]. Ultimately, however, the operational community seeks a better predictive capability. *Marcos et al.* [1998] have shown that the most likely route to this goal is through better solar EUV inputs to the models, such as that by *Lean et al.* [2001]. Under funding by the NASA Living With a Star Program, we are now pursuing this approach.

Appendix A: NRLMSISE-00 Formulation, Constraints, Generation, and Distribution Package

A1. Formulation

[55] The MSIS-class model formulation consists of parametric analytic approximations to physical theory for the vertical structure of the atmosphere as a function of location, time, solar activity (10.7-cm solar radio flux), and geomagnetic activity [*Hedin*, 1987]. Extending from the ground to the exobase, the NRLMSISE-00 model provides altitude profiles of temperature $T(z)$, number densities of species (He, O, N_2, O_2, Ar, H, N) in equilibrium at the temperature $T(z)$, total mass density $\rho(z)$, and the number density of a high-altitude "anomalous oxygen" component of total mass density that is not in thermal equilibrium at $T(z)$.

[56] For the thermosphere, the value of the total mass density at high altitude is the sum of two factors. The standard model subroutine (GTD7) always computes the "thermospheric" mass density by explicitly summing the masses of the species in equilibrium at the thermospheric temperature $T(z)$. A separate subroutine (GTD7D) computes the "effective" mass density by summing the thermospheric mass density and the mass density of the anomalous oxygen component. Below 500 km, the effective mass density is equivalent to the thermospheric mass density, and we drop the distinction.

[57] The model accounts for the approximate spheroidal symmetry of the Earth and the atmosphere by incorporating a gravity field and an effective Earth radius which are both latitude-dependent and by using spherical harmonics to represent spatial variability of the key parameters that define temperature and species number density profiles. Parameterized correction factors account for deviations of the profiles from the basic approximations in the lower thermosphere. Constraints on mixing ratio, hydrostatic equilibrium, and profile smoothness govern the transition between the thermosphere and the mesosphere.

A1.1. Thermosphere

[58] In the thermosphere, the Bates-Walker equations [*Walker*, 1965] represent the basic profiles of the temperature and of species number density as analytic functions of altitude. These equations are an exact solution for thermal and diffusive equilibrium and include thermal diffusion. Below a species-dependent altitude in the range 160–450 km, the profiles differ from diffusive equilibrium by progressively greater amounts as z decreases, transitioning to a fully mixed state at a turbopause $z_h \sim 100$ km. In this transition region, MSIS-class models modify the density profile due to the effects of chemistry, dynamics, and "loss/flow" processes.

[59] The appendix of *Hedin* [1987] gives the details on the thermospheric portion of the MSIS-class models, for which the fundamental variable is the temperature $T(z)$. The Bates-Walker temperature profile variables are the exospheric temperature $T_{\rm ex}$; the temperature at $z_{\rm lb} \equiv 120$ km, T_{120}; and the temperature gradient at $z_{\rm lb}$. These variables have the form (e.g., for T_{120})

$$T_{120} = \overline{T}_{120}[1 + G_{120}(L)],$$

where the overbar signifies a global and temporal mean and the function $G(L)$ includes time-independent terms, spherical harmonic terms, and time-dependent low-order harmonic terms. The spatial and temporal components are usually coupled, and the coefficients and phases represent the major spatial and temporal timescales inherent in the data. In addition, $G(L)$ contains polynomial terms in the solar EUV proxy ($F_{10.7}$ and $\langle F_{10.7}\rangle$, the 81-day average) and linear and exponential terms in geomagnetic activity. For chemical species i, the Bates-Walker profile variable is the number density at 120 km:

$$n_i = \overline{n}_i \exp[G_i(L)].$$

The subscript on G distinguishes among unique coefficient sets for respective thermospheric variables in the model.

[60] The NRLMSISE-00 model incorporates the following modifications of the equations in *Hedin* [1987]:

1. The solar EUV dependence includes a new cross term with coefficient B $\neq$ 0:

$$G(\text{solar}) = A\Delta F(1 + B\Delta\langle F\rangle) + C(\Delta F)^2 + D\Delta\langle F\rangle + E(\Delta\langle F\rangle)^2,$$

where $\Delta\langle F\rangle = \langle F_{10.7}\rangle - 150$, and $\Delta F = F_{10.7} - \langle F_{10.7}\rangle$, and $\langle F_{10.7}\rangle$ is the 81-day time-centered average of the 10.7-cm radio flux ($F_{10.7}$). In the definition of ΔF, $F_{10.7}$ is the previous day value of the radio flux.

2. The anomalous oxygen model profile, $[O_a](z)$, represents nonthermal oxygen species (e.g., O^+ and hot oxygen) inherent in the Jacchia and Barlier data sets at higher altitudes ($\geq$600 km) and is similar to an ionospheric Chapman layer [e.g., *Cotton et al.*, 1993]:

$$[O_a](z) = [O_a](z_{\rm lb}) \exp\left\{-\frac{\xi(z, z_{\rm lb})}{H(z_{\rm lb}, T_a)}\right\} \exp \cdot\left\{\frac{C}{H(z_a, T_a)}\left[1 - \exp\left(-\frac{z - z_a}{C}\right)\right]\right\},$$

where the geopotential height is $\xi(z, z_{\rm lb}) \approx z - z_{\rm lb}$, the scale height is, $H(z, T) \equiv [kT/mg(z)]$ (m is the mass of atomic oxygen), and the constants are $C = 76$ km, $z_a = 550$ km, $T_a = 4000$ K, $z_{\rm lb} = 120$ km, and $[O_a](z_{\rm lb})$ (set by data) = 6.0×10^4 cm^{-3}

3. Equations (A20a) and (A20b) of *Hedin* [1987] define a lower thermospheric density multiplier C_1 in equation (A12a); the purpose of this factor is to simulate chemistry and dynamic flow effects on various species. For [O] and [O_2] this factor now takes the form

$$C_1 = \exp\left\{\frac{R}{1 + \frac{1}{2}\{\exp[(z - z_c)/H_{c1}] + \exp[(z - z_c)/H_{c2}]\}}\right\},$$

where $R = R_c(1 + a_f\Delta\langle F\rangle)$. The constants are $R_c(O) = -0.076$, $R_c(O_2) = -0.75$, $a_f = 0.031$, $H_{c1}(O) = -H_{c1}(O_2) = 34.5$ km, $H_{c2}(O) = -H_{c2}(O_2) = 12.9$ km, and $z_c(O) = z_c(O_2) = 126.5$ km. (Note that the scale height variables H_{ci} have opposite signs to fit data on total oxygen content, [O] + 2[O_2].)

4. Consistent with *Banks and Kockarts* [1973], the thermal diffusion factors in NRLMSISE-00 are $\alpha_i = -0.38$ (i = He, H), 0.17 (i = Ar), 0.0 (other species). This represents a change from MSISE-90, which had $\alpha_i = -0.4$ (i = He, H) and 0.0 (other species). *Pavlov* [1979; private communication, 1998] suggests the following values: −0.38 (H), −0.28 (H_2), −0.27 (He), 0.17 (Ar), 0.12 (O_2), −0.08 (O), and 0.1 (N_2).

A1.2. Mesosphere

[61] The NRLMSIS database contains primarily data on total mass density and temperature in the upper mesosphere; even these data are notably sparse [*Hedin*, 1991]. For composition, the model primarily provides a smooth connection between the lower thermosphere and the region below 62.5 km, where ground-level mixing ratios are maintained. The dearth of data, coupled with extension of constraints (section A2) and the manner in which molecular oxygen is now represented in the new model, has combined to produce new capabilities and effects. The subsections below discuss two aspects of the new model.

A1.2.1. Mesosphere Inversion Layer

[62] Mesosphere inversion layers are regions of enhanced temperature ($\Delta T \sim 15$–50 K) which have been observed in two altitude regions in the mesosphere at low and middle latitudes and primarily at night [*Meriwether and Gardner*, 2000]. Present theory attributes the phenomenon to enhancement of tidal structure through interaction with gravity waves; a more comprehensive database of 24-hour observa-

tions in the mesosphere and lower thermosphere is necessary to confirm and complete the theory. Quantitative analysis of the MIL phenomenon is well beyond the scope of the present paper and the empirical model; here we merely point out NRLMSISE-00 does exhibit the shape of an upper MIL near the mesopause at low latitudes during nighttime. Under these conditions, this feature is more prominent in the new model than in MSISE-90 and therefore warrants mention. The structure becomes less apparent at midlatitudes, covers a broader altitude range, and appear to be less prominent at midnight than do the annual mean upper MIL profiles shown by Meriwether and Gardner. In this region, the NRLMSIS database contains only a few rocket observations (~60 temperature values), which do not appear to have sufficient information to cause this behavior in the model. On the other hand, the formulation is sufficiently flexible to capture statistically averaged MIL structures from data sets. Outside of the addition of new Millstone Hill Lower Thermosphere Coupling Study data in the 100- to 130-km altitude range, the only major difference from the MSISE-90 model is the imposition of hydrostatic equilibrium over a wider range (80–300 km; see section A2 below). The latter factor plus the lower-order tides in the model apparently have acted in concert to produce an MIL-like structure. Generating realistic MIL profiles with NRLMSIS awaits upgrading the model with the recent, extensive database of ground- and space-based observations of the upper mesosphere and mesopause.

A1.2.2. Molecular Oxygen (O_2) in the Mesosphere

[63] Section 4.2 of this paper shows that the SMM O_2 data have driven the NRLMSISE-00 thermospheric O_2 number density significantly lower than that of MSISE-90. Depending on the value of $\langle F_{10.7} \rangle$, this causes the increase of the NRLMSIS O_2 mixing ratio from the lower thermospheric value to the constant value (below 62.5 km) to be more gradual than that of MSISE-90, causing a lower O_2 mixing ratio (by up to a few percent) in the mesosphere. The dearth of data on mesospheric $[O_2]$ in the NRLMSIS database renders the selection of the NRLMSISE-00 or the MSISE-90 O_2 mixing ratio arbitrary at this time. Meanwhile, since the total mass density (ρ) in the mesosphere is credible, we suggest that users apply their mixing ratios of choice to ρ in order to estimate total oxygen content or O_2 mixing ratio in that region. As with the MIL phenomenon, the NRLMSIS formulation is sufficiently robust (or can be modified) to fit any data or constraints deemed appropriate by the mesospheric research community.

A2. Constraints

[64] For altitudes $0 \leq z < z_{lb} = 120$ km, the fundamental variables define nodes and gradients of the temperature profile, while pressure and density are defined by hydrostatic equilibrium and the ideal gas law [*Hedin*, 1991]. As was mentioned above, diffusive equilibrium no longer holds for the MSIS-class models below altitudes of ~300 km. Because we fit the temperature and individual species separately (different coefficient sets), the MSIS-class models do not maintain hydrostatic equilibrium a priori below 300 km. For this reason, the model generation process imposes an approximate hydrostatic equilibrium constraint in the region 80–300 km. This couples the lower and upper atmospheric regions, modifying some details of previous MSIS versions. Finally, since all of the new data relate to the thermosphere, NRLMSISE-00 retained the MSISE-90 coefficients below 72.5 km while constraining coefficient values in the range 72.5–110 km to give a total mass density at the ground in agreement with MSISE-90.

A3. Model Generation

[65] Generating a new version of the model requires calculation of optimal values for the ~2200 nonzero coefficients. Even though only a subset of the MSIS database is used to evaluate the model coefficients [*Hedin et al.*, 1977], the number of data points is still quite sizable ($\sim 3 \times 10^5$), rendering an all inclusive Levenberg-Marquardt calculation [*Press et al.*, 1992] compute-intensive and cumbersome. Because the NRLMSIS thermospheric data are separable by mass number (species, temperature, total mass density), one can partition the process into a series of separate Levenberg-Marquardt (LM) χ^2 minimization calculations for coefficient and data subsets covering different altitude regions, species, magnetic activity levels, and scales and types of variability. Each complete series of LM coefficient calculations (presently numbering 52) constitutes one "grand" fitting cycle. The grand cycles repeat until the coefficient set is stable [*Hedin*, 1987]. This approach has minimized memory requirements and maximized computing speed. We eliminate severe outliers by selecting only data points whose residuals are less than a specified multiple (6–15) of the observational uncertainty.

[66] The new drag and accelerometer data represent a significant departure from the above picture. In the present case, the total mass density provided by the model is a secondary or inferred quantity, given by the sum of species mass densities, in theory requiring that all of the species coefficients vary simultaneously to fit the data, which are extensive. To avoid this and other procedural difficulties, one can take advantage of the fact that different thermospheric species dominate the mass density in different altitude regions. Specifically, for N_2, O, and He, we have used the MSISE-90 model to determine the altitude ranges where the respective mass fractions are greater than 50%, thereby splitting the data into subsets. We have added these data subsets to the databases supporting the individual species coefficients and have combined the calculations of coefficients for N_2 and exospheric temperature (T_{ex}). As was described in section 4.1, we have extracted the high-altitude ($\geq$600 km) Jacchia and Barlier data to compute the coefficients associated with anomalous oxygen species and have excluded the summer high-altitude Jacchia and Barlier data in determining the standard thermospheric constituents.

A4. Distribution Package and Access

[67] The present NRLMSISE-00 distribution package is an ASCII file containing the model source, a test driver, and the expected output of the test driver. Users may acquire the file via two methods: (1) download from our website (http://uap-www.nrl.navy.mil/models_web/msis/msis_home.htm); (2) send e-mail to NRLMSISE-00@uap2.nrl.navy.mil (no subject or message), which will result in a reply with the file as an attachment.

[68] **Acknowledgments.** The authors gratefully acknowledge primary support by the Office of Naval Research, early support for one of us (A. Hedin) by the NASA Supporting Research and Technology Program, and

recent support by the NASA Living With a Star Program. Robert Meier receives credit for the vision and strong encouragement to continue development of the MSIS-class models. Generously providing new data sets and vital assistance to us were the following: Frank Marcos (Air Force Research Laboratory, accelerometer data); Francois Barlier (drag data, including those of Jacchia); Steven Cariglia, John Holt, Joseph Salah, and Michael Buonsanto (Millstone Hill, MIT Haystack Observatory, T_{ex}); Joseph Salah and Larisa Goncharenko (Millstone Hill, MIT Haystack Observatory, Lower Thermosphere Coupling Study, $T_{100-130}$); and Michael Sulzer and the CEDAR Database (Arecibo, T_{ex}). Millstone Hill, through its staff members John Holt, Michael Buonsanto, and Steven Cariglia, kindly invited and trained our research associate Owen Kelley, who retrieved T_{ex} from both the Millstone Hill and the Arecibo data sets in the Madrigal Database. The data provided by the Millstone Hill incoherent scatter radar were obtained under a National Science Foundation cooperative agreement with MIT, ATM-9714593. Robert Meier performed extensive testing of the new model in spectral inversion and data-fitting codes, and John Mariska, John Holt, James Bishop and Judith Lean tested the distribution package on a number of operating systems. We have also received invaluable guidance from William Oliver, James Bishop, Daniel Melendez-Alvira, Raymond Roble, Anatoli Pavlov, David Siskind, and Scott Budzien.

[69] Arthur Richmond thanks Hans G. Mayr and another reviewer for their assistance in evaluating this paper.

References

Aikin, A. C., A. E. Hedin, D. J. Kendig, and S. Drake, Thermospheric molecular oxygen measurements using the ultraviolet spectrometer on the Solar Maximum Mission spacecraft, *J. Geophys. Res.*, *98*, 17,607–17,613, 1993.

Arduini, C., U. Ponzi, and G. Laneve, Tidal analysis of the San Marco V and San Marco III: Density data in equatorial orbit, *J. Atmos. Sol. Terr. Phys.*, *59*(13), 1491–1503, 1997.

Banks, P. M., and G. Kockarts, *Aeronomy, Part B*, Academic, San Diego, Calif., 1973.

Barlier, F., C. Berger, J. L. Falin, G. Kockarts, and G. Thuillier, A thermospheric model based on satellite drag data, *Ann. Geophys.*, *34*, 9–24, 1978.

Boudon, Y., F. Barlier, A. Bernard, R. Juillerat, and A. Mainguy, Synthesis of flight results of the CACTUS accelerometer for accelerations below 10−9g, *Acta Astronaut.*, *6*(11), 1387–1398, 1979.

Buonsanto, M. J., and L. M. Pohlman, Climatology of neutral exospheric temperature above Millstone Hill, *J. Geophys. Res.*, *103*, 23,381–23,392, 1998.

Champion, K. S. W., and F. A. Marcos, The triaxial-accelerometer system on Atmosphere Explorer, *Radio Sci.*, *8*(4), 297–303, 1973.

Cotton, D. M., G. R. Gladstone, and S. Chakrabarti, Sounding rocket observation of a hot atomic oxygen geocorona, *J. Geophys. Res.*, *98*, 21,651–21,657, 1993.

Goncharenko, L. P., and J. E. Salah, Climatology and variability of the semidiurnal tide in the lower thermosphere over Millstone Hill, *J. Geophys. Res.*, *103*, 20,715–20,726, 1998.

Gonzalez, S. A., and M. P. Sulzer, Detection of He^+ Layering in the topside ionosphere over Arecibo during equinox solar minimum conditions, *Geophys. Res. Lett.*, *23*(18), 2509–2512, 1996.

Hedin, A. E., MSIS-86 thermospheric model, *J. Geophys. Res.*, *92*, 4649–4662, 1987.

Hedin, A. E., High altitude atmospheric modeling, *NASA Tech. Memo.*, *100707*, 1988.

Hedin, A. E., Hot oxygen geocorona as inferred from neutral exospheric models and mass spectrometer measurements, *J. Geophys. Res.*, *94*, 5523–5529, 1989.

Hedin, A. E., Extension of the MSIS thermosphere model into the middle and lower atmosphere, *J. Geophys. Res.*, *96*, 1159–1172, 1991.

Hedin, A. E., et al., A global thermospheric model based on Mass Spectrometer and Incoherent Scatter data MSIS 1: N_2 density and temperature, *J. Geophys. Res.*, *82*, 2139–2147, 1977.

Jacchia, L., New static models of the thermosphere and exosphere with empirical temperature profiles, *Spec. Rep. 313*, Smithsoni. Astrophys. Observ., Cambridge, Mass., May 6, 1970.

Kayser, D. C., Solar flux variation of the thermospheric molecular oxygen density, *J. Geophys. Res.*, *85*, 695–702, 1980.

Keating, G. M., J. C. Leary, B. D. Green, O. M. Uy, R. C. Benson, R. E. Erlandson, T. E. Phillips, J. C. Lesho, and M. T. Boies, Neutral and ion drag effects near the exobase: MSX satellite measurements of He and O^+, in *Astrodynamics 1997: Advances in the Astronautical Sciences*, vol. 97(1), edited by F. Hoots, B. Kaufman, P. Cefola, and D. Spencer, pp. 549–556, Am. Astronaut. Soc., San Diego, Calif., 1998.

Knowles, S. H., J. M. Picone, S. Thonnard, and A. Nicholas, The effect of atmospheric drag on satellite orbits during the Bastille Day event, *Sol. Phys.*, *204*, 387–397, 2001.

Lean, J. L., O. R. White, W. C. Livingston, and J. M. Picone, Variability of a composite chromospheric irradiance index during the 11-year activity cycle and over longer time periods, *J. Geophys. Res.*, *106*, 10,645–10,658, 2001.

Litvin, A., W. L. Oliver, J. M. Picone, and M. J. Buonsanto, The upper atmosphere during 5–11 June 1991, *J. Geophys. Res.*, *105*, 12,789–12,796, 2000.

Marcos, F. A., A. E. Hedin, J. Liu, J. N. Bass, and C. R. Baker, Operational satellite drag model standards, in *33rd Aerospace Sciences Meeting and Exhibit, Reno, Nevada*, Am. Inst. of Aeronaut. and Astronaut., New York, 1995.

Marcos, F. A., M. J. Kendra, J. M. Griffin, J. N. Bass, D. R. Larson, and J. J. F. Liu, Precision low Earth orbit determination using atmospheric density calibration, in *Astrodynamics 1997: Advances in the Astronautical Sciences*, vol. 97(1), edited by F. Hoots, B. Kaufman, P. Cefola, and D. Spencer, pp. 501–513, Am. Astronaut. Soc., San Diego, Calif., 1998.

Meier, R. R., J. M. Picone, D. P. Drob, and R. G. Roble, Similarity transformation-based analysis of atmospheric models, data, and inverse remote sensing algorithms, *J. Geophys. Res.*, *106*, 15,519–15,532, 2001.

Melendez-Alvira, D. J., J. M. Picone, O. A. Kelley, Q. Zhou, and M. P. Sulzer, Histograms of Arecibo World Days measurements and linear-H fits between 1985 and 1995, *NRL Memo. Rep. NRL/MR/7640-98-831*, Nav. Res. Lab., Washington, D. C., 1998.

Meriwether, J. W., and C. S. Gardner, A review of the mesosphere inversion layer phenomenon, *J. Geophys. Res.*, *105*, 12,405–12,416, 2000.

Neal, H. L., S. L. Coffey, and S. Knowles, Maintaining the space object catalog with special perturbations, in *Astrodynamics 1997: Advances in the Astronautical Sciences*, vol. 97(2), edited by F. Hoots, B. Kaufman, P. Cefola, and D. Spencer, pp. 1349–1360Am. Astronaut. Soc., San Diego, Calif., 1998.

Nicholas, A., J. M. Picone, S. E. Thonnard, R. R. Meier, K. F. Dymond, and D. P. Drob, A methodology for using optimal MSIS parameters retrieved from SSULI data to compute satellite drag on LEO objects, *J. Atmos. Sol. Terr. Phys.*, *62*, 1317–1326, 2000.

Oliver, W. L., Hot oxygen and the ion energy budget, *J. Geophys. Res.*, *102*, 2503–2511, 1997.

Oliver, W. L., and J. Schoendorf, Variations of hot O in the thermosphere, *Geophys. Res. Lett.*, *26*(18), 2829–2832, 1999.

Pavlov, A. V., Thermal diffusion in the upper atmosphere of the Earth, *Geomagn. Aeron.*, *19*(6), 707–711, 1979.

Press, W. H., S. A. Teukolsky, W. T. Vetterling, and B. P. Flannery, *Numerical Recipes: The Art of Scientific Computing*, Cambridge Univ. Press, New York, 1992.

Rhoden, E. A., J. M. Forbes, and F. A. Marcos, The influence of geomagnetic and solar variabilities on lower thermosphere density, *J. Atmos. Sol. Terr. Phys.*, *62*, 999–1013, 2000.

Schoendorf, J., L. A. Young, and W. L. Oliver, Hot oxygen profiles for incoherent scatter radar analysis of ion energy balance, *J. Geophys. Res.*, *105*, 12,823–12,832, 2000.

Walker, J. C. G., Analytic representation of upper atmosphere densities based on Jacchia's static diffusion models, *J. Atmos. Sci.*, *22*, 462–463, 1965.

Yee, J. H., J. W. Meriwether Jr., and P. B. Hays, Detection of a corona of fast oxygen atoms during solar maximum, *J. Geophys. Res.*, *85*, 3396–3400, 1980.

A. C. Aikin, Laboratory for Extraterrestrial Physics, NASA Goddard Space Flight Center, Greenbelt, MD 20771, USA.

D. P. Drob, A. E. Hedin, and J. M. Picone, Naval Research Laboratory, Space Science Division, Code 7643, Building 209, 4555 Overlook Avenue, SW, Washington, D. C. 20375-5320, USA. (picone@nrl.navy.mil)